31st Annual International Conference of the IEEE EMBS
Minneapolis, Minnesota, USA, September 2-6, 2009

# Electrical conductivity imaging using magnetic resonance tomography

Ulrich Katscher, Tobias Voigt, and Christian Findeklee

*Abstract*— **The electrical conductivity of human tissue could be used as an additional diagnostic parameter or might be helpful for the prediction of the local SAR during MR measurements. In this study, the approach "Electric Properties Tomography" (EPT) is applied, which derives the patient's electric conductivity using a standard MR system. To this goal, the spatial transmit sensitivity distribution of the applied RF coil is measured. This sensitivity distribution represents the positive circularly polarized component of the magnetic field. It can be post-processed utilizing Faraday's and Ampere's law, yielding an estimation of the spatial distribution of the patient's electric conductivity. Thus, EPT does not apply externally mounted electrodes, currents, or RF probes. In this study, phantom experiments underline the principle feasibility of EPT. Furthermore, initial conductivity measurements in the brain allow distinguishing cerebro-spinal fluid from the surrounding grey and white matter.**

## I. Introduction

THE electric properties of the human body, i.e., the electric conductivity $\sigma$ and permittivity $\varepsilon$, characterize various kinds of healthy (see, e.g., [1,2]) as well as pathologic tissue. The most prominent example in this framework might be the pathological alteration of $\sigma$ and $\varepsilon$ in tumours [3-7]. Besides diagnosis, $\sigma$ is a key factor for the Specific energy Absorption Rate (SAR), which is a major problem in today's high-field MR.

A well-known method of measuring electric properties *in vivo* is Electric Impedance Tomography (EIT) (see, e.g., [8-13]). EIT is based on low-frequency currents, which are applied to the human body via external electrodes [11] or induced by suitable RF coils [12]. A different method is given by measuring the applied currents via MR phase imaging yielding "current density imaging" [14,15] or "MR-EIT" [16,17].

The approach of the current paper, called Electric Properties Tomography (EPT) [18,19], differs from the presented approaches substantially. It is based on standard B1-mapping, i.e. measuring the active magnetic component of the applied RF field (see, e.g., [20-23]). Hence, no electrode mounting is required, and the energy deposited in the human body is the same as for standard MR imaging. No inverse problem has to be solved, and the spatial resolution is given by the resolution of the MR image and the quality of the applied B1-mapping technique. In opposite to an earlier version of EPT [18,19], the explicit calculation of the electric field is not required due to the introduction of certain model assumptions. Instead, an estimation of the electric field is obtained as an additional output of EPT.

The electric conductivity depends on the frequency of the applied RF field. With EPT, the conductivity is determined at the Larmor frequency corresponding to the main field of the MR system used, which in this study is 64 MHz.

The paper first derives the central equation of EPT. Then, the steps necessary to solve this equation are discussed. Corresponding phantom experiments are performed investigating different conductivities reflecting the range of human tissue conductivities. Finally, initial *in vivo* results are shown.

Manuscript received April 6, 2009.

U. Katscher and C. Findeklee are with Philips Research Europe-Hamburg, Sector Medical Imaging Systems, 22335 Hamburg, Germany (Phone and e-mail of corresponding author +49-40-5078-2334, ulrich.katscher@philips.com).

T. Voigt is with the Institute of Biomedical Engineering, University of Karlsruhe, 76128 Karlsruhe, Germany.

## II. Theory

### A. Derivation of central EPT equation

Faraday's law in integral form is given by

$$-i\omega\mu\int_A \mathbf{H}(\mathbf{r})\cdot \mathrm{d}\mathbf{a} = \oint_{\partial A} \mathbf{E}(\mathbf{r})\cdot \mathrm{d}\mathbf{l} \qquad (1)$$

with $\omega$ the Larmor frequency, $\mu$ the (assumed to be constant) permeability, $A$ the integration area, and $\partial A$ the curve around the integration area. The magnetic field strength **H** and the electric field **E** are assumed to be time-harmonic **H,E** ~ exp($i\omega t$). On the other hand, Ampere's law in differential form for time-harmonic fields can be written as

$$\nabla\times\mathbf{H}(\mathbf{r})/i\omega = \kappa(\mathbf{r})\mathbf{E}(\mathbf{r}) \ . \qquad (2)$$

Here, $\kappa = \varepsilon - i\sigma/\omega$ denotes the (assumed to be isotropic) complex permittivity, $\varepsilon$ the real permittivity, and $\sigma$ the electric conductivity. To estimate $\kappa$, (2) is integrated around $\partial A$ and divided by (1)

$$\frac{\oint_{\partial A}\nabla\times\mathbf{H}(\mathbf{r})\cdot\mathrm{d}\mathbf{l}}{\mu\omega^2\int_A \mathbf{H}(\mathbf{r})\cdot\mathrm{d}\mathbf{a}} = \frac{\oint_{\partial A}\kappa(\mathbf{r})\mathbf{E}(\mathbf{r})\cdot\mathrm{d}\mathbf{l}}{\oint_{\partial A}\mathbf{E}(\mathbf{r})\cdot\mathrm{d}\mathbf{l}} \approx \kappa(\mathbf{r}) \ . \qquad (3)$$

This estimation is valid in regions, where the spatial variation of $\kappa$ along $\partial A$ is significantly smaller than the variation of **E**

$$\left.\frac{\delta\kappa(\mathbf{r})}{\delta\mathbf{E}(\mathbf{r})}\right|_{\partial A} << 1 \ , \qquad (4)$$

which is fulfilled, e.g., inside compartments with constant $\kappa$. Equation (3) provides an estimation of $\kappa$, which requires only the knowledge of the three spatial components of the magnetic field. Due to assumption (4), the knowledge of the electric field is not required explicitly in contrast to earlier versions of EPT [18,19]. However, regarding the magnetic RF field, only the components perpendicular to the main field $B_o$ influence MR images. Thus, in principle, only the perpendicular components seem to be detectable with MR, but not the component parallel to $B_o$ (usually called $z$-direction). This feature makes it advantageous to choose a non-transverse integration area $A$ to avoid the division by $H_z$ in (3). For instance, (3) reads for a coronal area $A=A_{xz}$

$$\frac{\oint_{\partial A_{xz}} \left\{\left(\partial_y H_z - \partial_z H_y\right), \left(\partial_x H_y - \partial_y H_x\right)\right\} \cdot \mathrm{d}\mathbf{l}}{\mu\omega^2 \int_{A_{xz}} H_y \,\mathrm{d}x\mathrm{d}z} \approx \kappa(\mathbf{r}) \,. \qquad (5)$$

A coronal integration area suggests the imaging of coronal slices to facilitate numerics, however, it can also be implemented for non-coronal imaging slices.

Please note that (5) provides absolute values of $\kappa$ even in the case that only relative values of the magnetic field are measured.

### *B. Determination of the main magnetic field component*

For EPT, Eq. (5) is applied to a transmit/receive RF coil of a standard MR system. Thus, the quantities $H_x$, $H_y$, and $H_z$ of the involved RF coil have to be determined.

During RF transmission in MRI, only the positive circularly polarized magnetic field component $H^+ = (H_x+iH_y)/2$ is active. It can be measured with so-called B1 mapping techniques (see, e.g., [20-23]). For a standard quadrature coil for RF transmission, $H^+$ is the dominant component, i.e., $H^- = (H_x - iH_y)/2 << H^+$ and $H_z << H^+$. Thus, this study assumes $H^- \equiv H_z \equiv 0$, and Eq. (5) can be re-written

$$\frac{-\oint_{\partial A_{xz}} \left\{\left(\partial_z H^+\right), \left(i\partial_x H^+ + \partial_y H^+\right)\right\} \cdot \mathrm{d}\mathbf{l}}{\mu\omega^2 \int_{A_{xz}} H^+ \,\mathrm{d}x\mathrm{d}z} \approx \kappa(\mathbf{r}) \,, \qquad (6)$$

which turns out to be the central equation of this study. Please note that the discussed assumption $H^- \equiv H_z \equiv 0$ is optimally fulfilled for quadrature body or head coils. The use of other RF coils typically violates this assumption, yielding suboptimal reconstruction results, and thus, is not recommended for EPT.

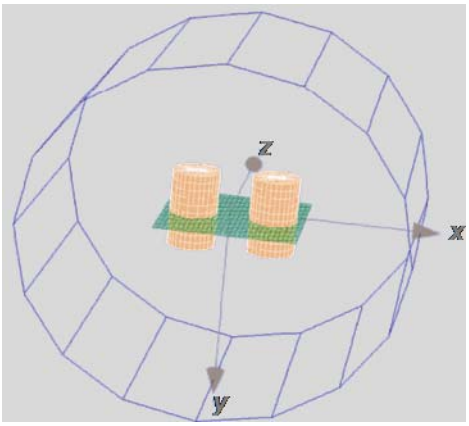


Fig. 1 Set up of the phantom experiments. Blue: RF body coil, orange: bi-cylindrical phantom, green: coronal imaging slice.

## III. Methods

EPT was applied to an iso-centric, bi-cylindrical phantom (diameters = 7.5cm, height = 13cm, cylinder axis distance = 12.5 cm) with different electric conductivities in a quadrature body coil at 64 MHz (see Fig. 1). The phantom was filled with different saline solutions between 0.05 S/m to 5.0 S/m, covering the physiological range [1,2]. The conductivities were checked prior to the MRI experiment using a 4-ring potentiometric probe (HI8733, Hanna Instruments, USA). To enhance the MR signal, 2 ml Magnevist (Bayer Schering Pharma AG, Berlin, Germany) was added per liter saline solution. Experiments were performed on a Philips Achieva 1.5T system (Philips Medical Systems, Best, The Netherlands). B1 maps were acquired using "Actual Flip angle Imaging" (AFI) [22,23]. A 3D sequence with TR1 = 32 ms, TR2 = 160 ms, TE = 2.5 ms, a spatial resolution=1.15×1.15×8 mm, coronal slice orientation, and a nominal flip angle of $\alpha = 60°$ was used. The same sequence was used to image the head of a volunteer. To reconstruct $\sigma$ via Eq. (6), a coronal integration area was chosen. The required differentiations were performed via Savitzky-Golay filtering [24].

## IV. Results / Discussion

First, the phantom was investigated with saline concentrations yielding conductivities of 0.47 S/m and 2.14 S/m. Fig. 2 shows the obtained experimental reconstruction results yielding mean conductivities in the two cylinders of 0.45±0.038 S/m and 1.92±0.059 S/m.

Second, the experiment was repeated using 10 different conductivities between 0.05 S/m and 5.0 S/m in one of the cylinders, reflecting the physiological range of conductivities [1,2]. A high correlation of 99.6% was found between conductivities measured a priori and with EPT (see Fig. 3).

Finally, EPT was applied to the head of the volunteer (Fig. 4). Here, a significant contrast between the cerebrospinal fluid (CSF) in the lateral ventricles and the surrounding white matter is visible. Accordingly, the sub-cranial CSF

yields a significant image contrast. The reconstructed mean conductivity in the different CSF compartments is roughly 3.3 S/m, which is comparable to the literature value of 2.1 S/m [1,2]. In the brain, the reconstructed mean value is roughly 0.34 S/m, which again is comparable to literature values (0.51 S/m for grey and 0.29 S/m for white matter [1,2]).

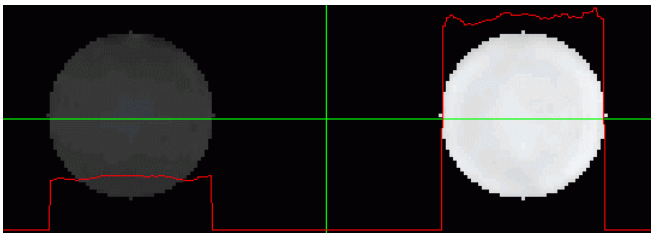

Fig. 2 Reconstructed phantom conductivity. The mean values are 0.45±0.038 S/m in the left cylinder (a priori measurement = 0.47 S/m) and 1.92±0.059 S/m in the right cylinder (a priori measurement = 2.14 S/m).

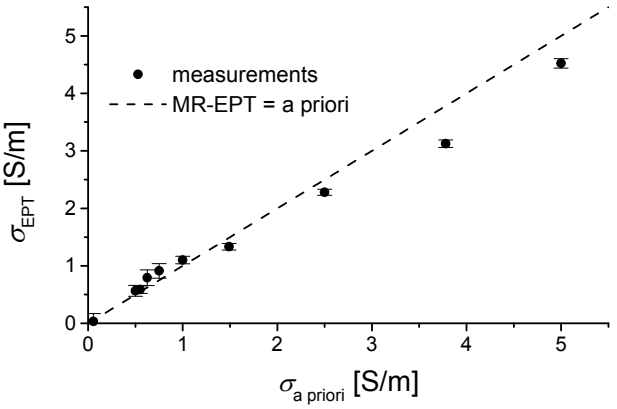


Fig. 3 Mean phantom conductivities determined with EPT as a function of the conductivities measured *a priori* with an independent probe. The correlation between the two quantities is 99.6%.

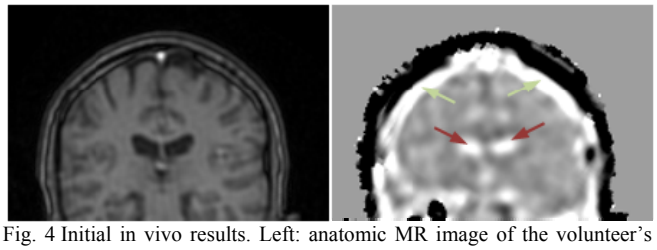

Fig. 4 Initial in vivo results. Left: anatomic MR image of the volunteer's head. Right: reconstructed conductivity. A clear contrast between ventricular / sub-cranial CSF (red / green arrows) and the surrounding gray / white matter is visible.

## V. Summary / Conclusion

The presented results of the EPT experiments highly correlate with the expected values, underlining the principle feasibility of EPT. The approach seems to be able to detect the electric conductivity quantitatively with a standard MR system. Future studies will further investigate the *in vivo* feasibility of EPT, particularly in the framework of oncology.

## References


1. Gabriel C, Gabriel S, Courhout E (1996) The dielectric properties of biological tissues: I. Literature Survey. Phys Med Biol 41:2231-2249
2. Gabriel S, Lau RW, Gabriel C (1996) The dielectric properties of biological tissues: II. Measurements in the frequency range 10 Hz to 20 GHz. Phys Med Biol 41:2251–2269
3. Surowiec AJ, Stuchly SS, Barr JB et al. (1988) Dielectric properties of Breast Carcinoma and the Surrounding Tissues. IEEE Trans Biomed Eng 35:257-263
4. Lu Y, Li B, Xu J et al. (1992) Dielectric properties of human glioma and surrounding tissue. Int J Hyperthermia 8:755-760
5. Joines WT, Zhang Y, Li C et al. (1994) The measured electrical properties of normal and malignant human tissues from 50 to 900 MHz. Med Phys 21:547-550
6. Smallwood RH, Keshtkar A, Wilkinson BA et al. (2002) Electrical Impedance Spectroscopy (EIS) in the Urinary Bladder: The Effect of Inflammation and Edema on Identification of Malignancy. IEEE Trans Med Img 21:708-710
7. Haemmerich D, Staelin ST, Tsai JZ et al. (2003) In vivo electrical conductivity of hepatic tumours. Physiol Meas 24:251-260
8. Fuks LF, Cheney M, Isaacson D et al. (1991) Detection and imaging of electric conductivity and permittivity at low frequency. IEEE Trans Biomed Eng 38:1106-1110
9. Eyuboglu BM, Pilkington TC, Wolf PD (1994) Estimation of tissue resistivities from multiple-electrode impedance measurements. Phys Med Biol 39:1-17
10. Edic PM, Saulnier GJ, Newell JC et al. (1995) A Real-Time Elec-trical Impedance Tomograph. IEEE Trans Biomed Eng 42:849-859
11. Saulnier GJ, Blue RS, Newell JC et al. (2001) Electrical Impedance Tomography 2001. IEEE Sig Proc Mag 18:31-43
12. Gençer NG, Ider YZ, Williamson SJ. (1996) Electrical Impedance Tomography: Induced-Current Imaging Achieved with a Multiple Coil System. IEEE Trans Biomed Eng 43:139-149
13. Cherepenin V, Karpov A, Korjenevsky A et al. (2001) A 3D electrical impedance tomography (EIT) system for breast cancer detection. Physiol Meas 22:9-18
14. Scott GC, Joy MLG, Armstrong RL et al. (1991) Measurement of Nonuniform Current Density by Magnetic Resonance. IEEE Trans Med Img 10:362-374
15. Scott JC, Joy MLG, Armstrong RL et al. (1992) Sensitivity of Magnetic-Resonance Current-Density Imaging. J Magn Reson 97:235-254
16. Muftuler LT, Hamamura M, Birgul O, Nalcioglu O. (2004) Resolution and Contrast in Magnetic Reconance Electrical Impedance Tomography (MREIT) and its Application to Cancer Imaging. Techn Canc Res Treat 3:599-609
17. Seo JK, Kwon O, Woo EJ. (2005) Magnetic resonance electrical impedance tomography (MREIT); conductivity and current density imaging. J Phys Conf Ser 12:140-155
18. Katscher U, Hanft M, Vernickel P et al. (2006) Electric Properties Tomography (EPT) via MRI. Proc Intl Soc Mag Reson Med 14:3037
19. Katscher U, Hanft M, Vernickel P et al. (2006) Experimental verification of Electric Properties Tomography (EPT), Proc Intl Soc Mag Reson Med 14:3035
20. Akoka S, Franconi F, Seguin F et al. (1993) Radiofrequency map of an NMR coil by imaging. Magn Reson Imag 11:437-441
21. Stollberger R, Wach P. (1996) Imaging of the active B1 field in vivo. Magn Reson Med 35:246-251
22. Yarnykh VL. (2007) Actual flip-angle imaging in the pulsed steady state: a method for rapid three-dimensional mapping of the transmitted radiofrequency field. Magn Reson Med 57:192-200
23. Nehrke K. (2009) On the steady-state properties of actual flip angle imaging (AFI). Magn Reson Med 61:84-92
24. Press WH, Teukolsky SA, Vetterling WT, Flannery BP. (1995) Numerical Recipes in C. Cambridge University Press